4'-Fluorouridine mitigates lethal infection with pandemic human and highly pathogenic avian influenza viruses

Carolin M Lieber[1], Megha Aggarwal[1], Jeong-Joong Yoon[1], Robert M Cox[1], Julien Sourimant[1], Mart Toots[1], Hae-Ji Kang[1], Scott K Johnson[2], Cheryl A Jones[2], Zachary M Sticher[3], Alexander A Kolykhalov[3], Manohar T Saindane[3], Stephen M Tompkins[2], Oliver Planz[4], George R Painter[3], Michael G Natchus[3], Kaori Sakamoto[5], Richard K Plemper[1]*

[1]Center for Translational Antiviral Research, Georgia State University Institute for Biomedical Sciences, Atlanta, GA, 30303, USA.

[2]Center for Vaccines and Immunology, University of Georgia, Athens, GA, 30602, USA

[3]Emory Institute for Drug Development, Emory University, Atlanta, GA, 30329, USA

[4]Department of Immunology, Interfaculty Institute for Cell Biology, Eberhard Karls University Tübingen, Tübingen, Germany

[5]Department of Pathology, College of Veterinary Medicine, University of Georgia, Athens, GA, 30602, USA.

Keywords: influenza virus, pandemic preparedness, antiviral, nucleoside analog, 4'-Fluorouridine

*Corresponding author: rplemper@gsu.edu

Abstract

Influenza outbreaks are associated with substantial morbidity, mortality and economic burden. Next generation antivirals are needed to treat seasonal infections and prepare against zoonotic spillover of avian influenza viruses with pandemic potential. Having previously identified oral efficacy of the nucleoside analog 4'-Fluorouridine (4'-FIU, EIDD-2749) against SARS-CoV-2 and respiratory syncytial virus, we explored activity of the compound against seasonal and highly pathogenic influenza (HPAI) viruses in cell culture, human airway epithelium organoids, and/or two animal models, ferrets and mice, that assess IAV transmission and lethal viral pneumonia, respectively. 4'-FIU inhibited a panel of relevant influenza A and B viruses with nanomolar potency in organoids. *In vitro* polymerase assays revealed immediate chain termination of IAV polymerase after 4'-FIU incorporation, in contrast to delayed chain termination of SARS-CoV-2 and RSV polymerase. Once-daily oral treatment of ferrets with 2 mg/kg 4'-FIU initiated 12 hours after infection rapidly stopped virus shedding and prevented direct-contact transmission to untreated sentinels. Treatment of mice infected with a lethal inoculum of pandemic A/CA/07/2009 (H1N1)pdm09 (Ca09) with 2 mg/kg 4'-FIU alleviated pneumonia. Three doses mediated complete survival when treatment was initiated up to 60 hours after infection, indicating an unusually broad window for effective intervention. Therapeutic oral 4'-FIU ensured survival of animals infected with HPAI A/VN/12/2003 (H5N1) and of immunocompromised mice infected with pandemic Ca09. Recoverees were fully protected against homologous reinfection. This study defines the mechanistic foundation for high sensitivity of influenza viruses to 4'-FIU and supports 4'-FIU as developmental candidate for the treatment of seasonal and pandemic influenza.

Author Summary

Next-generation antiviral therapeutics are needed to better mitigate seasonal influenza and prepare against zoonotic virus spillover from animal reservoirs. At greatest risk are the immunocompromised and patients infected with highly pathogenic influenza viruses. In this study, we have demonstrated efficacy of a broad-spectrum nucleoside analog, 4'-fluorouridine, against a representative panel of influenza viruses in cell culture, human organoids, and two animal models,

ferrets and mice. Acting as an immediate chain terminator of the influenza virus polymerase, once-daily oral treatment protected against lethal infection with seasonal and highly pathogenic avian influenza viruses, prevented direct-contact transmission to untreated sentinels, and mitigated lethal infection of immunocompromised hosts. These results support the developmental potential of 4'-fluorouridine for treatment of vulnerable patient groups and mitigation of pandemic influenza, providing a much-needed additional therapeutic option for improved disease management.

Introduction

Influenza A viruses (IAV) are zoonotic negative sense, segmented RNA viruses with high pandemic potential [1]. Wild aquatic birds are a major natural reservoir for avian influenza viruses, creating high opportunity for spread into the poultry industry and spillover of HPAI viruses into the human population with potentially catastrophic consequences [2, 3]. The 2021-2022 H5N1 HPAID epidemic specifically is the largest on record, having reached an unprecedented geographical expansion and requiring the culling of 48 million birds so far [4]. Approximately 14 IAV pandemics have occurred in the past 500 years [5], six of which were concentrated in the last 120 years alone. Most deadly of these outbreaks was the 1918 "Spanish Flu" pandemic, which was caused by an H1N1 subtype IAV of unusual virulence that accounted for approximately 500 million infected people, equating to nearly a third of the world population at the time, and 50 million death [6]. Case fatality rates were particularly high in young children, 20-40 year old adults, and the elderly above 65 years of age [6]. Subsequent pandemics in the 20th century included the Asian influenza of 1957 and the Hong Kong influenza of 1968, which were caused by IAV of H2N2 and H3N2 subtypes, respectively [7], and the swine origin H1N1 outbreak of 2009 [8]. Although considered less pathogenic than several of the earlier pandemic strains, pdm09 IAV is still estimated to have caused 151,000 to 575,400 deaths worldwide and major economic damage [9].

Influenza viruses cause rapid-onset disease with high fever, cough, body aches, rhinorrhea, and nasal congestion [10]. Advance to severe disease is marked by virus invasion of the small airways and viral pneumonia, which can lead to sepsis due to a hyperinflammatory systemic response [11]. Other

serious complications include myocarditis, encephalitis, myositis, and multi-organ failure [12, 13]. At greatest risk of life-threatening influenza are children less than 2 years of age, older adults, pregnant women, and patients with pre-existing conditions such as asthma, diabetes, or chronic heart disease [14]. Vaccine prophylaxis is available, but the efficacy of the seasonal tetravalent influenza vaccine is moderate, ranging from 40 to 60% even under optimal conditions in interpandemic years [15]. Effectiveness of the vaccine can be substantially lower in older adults, who are at greatest risk of progressing to severe disease, or when vaccine components and circulating strains are poorly matched [15]. Multiple avenues are being pursued to develop a broad-spectrum influenza vaccine, but none have yet achieved regulatory approval [16].

To improve disease management especially in vulnerable patient groups, rapidly respond to endemic outbreaks of seasonal influenza when the vaccine is not optimally matched, and to prepare for the pandemic threat originating from zoonotic transmission of HPAI viruses, effective therapeutics with a higher barrier against viral resistance are urgently needed. Three classes of antiviral drugs have received approval by the FDA for treatment of influenza thus far. The M2 channel blocking adamantanes (amantadine and rimantadine), the neuraminidase inhibitors (oral oseltamivir, inhaled zanamivir, intravenous peramivir), and, most recently, the PA endonuclease inhibitor baloxavir marboxil [17]. Of these, use of the adamantanes has been discontinued due to widespread pre-existing resistance in human influenza viruses and natural IAV reservoirs [18]. Pre-existing signature resistance mutations against the neuraminidase inhibitors were furthermore detected in 2009 pandemic viruses [19], giving rise to the concern that future effectiveness of this inhibitor class may be questionable [20]. Although baloxavir marboxil is the newest influenza drug, resistance has developed rapidly and was even observed in human patients during the early clinical trials, resulting in rebound of virus replication [21-23]. Novel therapeutic options are therefore needed to broaden the available anti-influenza virus drug arsenal.

In search of suitable broad-spectrum developmental candidates, we explored in this study antiviral potency, *in vivo* efficacy, and mechanism of action of 4'-FIU against the influenza virus indication. Recently, we reported that 4'-FIU is a highly potent inhibitor of SARS-CoV-2 and pathogens of the

mononegavirus order [24, 25], establishing oral efficacy in animal models of SARS-CoV-2 and respiratory syncytial virus (RSV) infection. Having demonstrated that this nucleoside analog functions as an immediate chain terminator of influenza virus polymerase, we assessed oral efficacy in two different animal models, mice and ferrets, against pandemic human and HPAI viruses. Influenza treatment paradigms developed in these models outline an unusually broad time window for successful therapeutic interference with a lethal viral challenge. These results support the development of 4'-FIU as a therapeutic candidate for the treatment of influenza with the potential to improve preparedness against zoonotic spillover of avian IAVs with pandemic potential into the human population.

Results

To explore whether the indication spectrum of 4'-FIU (Fig 1a) extends to the orthomyxoviruses, we examined activity of the compound against seasonal and pandemic IAVs representing H1N1 and H3N2 subtypes and against a representative influenza B virus (IBV) isolate in cell culture (Fig 1b). In parallel, we generated human airway epithelium organoids grown at air-liquid interface from a healthy donor and tested inhibition of pandemic Ca09 through basolateral 4'-FIU (Fig 1c), and determined activity against a recombinant A/WSN/33 (H1N1)-based reporter virus [26] on non-differentiated primary HAE cells representing 10 distinct donors (S1 Fig). All viral isolates tested were highly sensitive to the compound, returning 50% and 90% inhibitory concentrations (EC_{50} and EC_{90}, respectively) in the nanomolar range with steep Hill slopes. Combined with a 50% cytotoxic concentration (CC_{50}) of 4'-FIU of 468 μM [24] in primary HAEs from the same donor as used in the organoid model, we calculated a selectivity index (SI = CC_{50}/EC_{50}) of 4'-FIU against pandemic Ca09 of 15,600 in this disease-relevant human tissue model.

4'-FIU is an immediate chain terminator of influenza virus polymerase

Through biochemical RdRP assays using purified recombinant RSV and SARS-CoV-2 polymerase complexes and synthetic template RNA, we have demonstrated that incorporation of 4'-FIU triphosphate (4'-FIU-TP) into nascent chain RNA triggers delayed termination of the RNA-dependent RNA polymerases from a negative sense (RSV) and a positive sense (SARS-CoV-2) RNA virus. Whereas variations in stalling efficiencies were observed between sequences and polymerase, position

i+3 marked the predominant stalling site [24]. Following expression of IAV RdRP PA, PB1, and PB2 subunits in insect cells, we subjected affinity chromatography purified, reconstituted IAV polymerase to the equivalent biochemical RdRP assay in the presence of increasing concentrations of 4'-FIU-TP or UTP (Figs 1d and 1e, S2a to S2e Figs). 4'-FIU-TP was incorporated instead of UTP when the polymerase reached the first adenosine in the template RNA as we had noted before in RSV and SARS-CoV-2 RdRP assays [24], but then triggered immediate chain termination of IAV RdRP. Densitometric quantitation of relative amplicon intensities to compare incorporation rates of the analog relative to UTP revealed an approximately 4-fold higher affinity of IAV polymerase for endogenous UTP than for 4'-FIU-TP (Fig 1f).

These results demonstrate high sensitivity of influenza virus polymerases to 4'-FIU and identify sequence-independent immediate chain termination at position *i* as a predominant mechanism of influenza virus RdRP inhibition by the compound.

Pharmacokinetic (PK) properties of 4'-FIU in mouse plasma and tissues

We have previously demonstrated oral bioavailability of 4'-FIU in ferrets and efficient intracellular anabolism to 4'-FIU-TP with prolonged tissue exposure levels [24]. To assess cross-species conservation of PK profiles between IAV efficacy models used in this study, ferrets and mice, we subjected the compound to a single-dose oral PK study in mice, measuring 4'-FIU plasma concentrations and corresponding 5'-triphosphate levels in selected soft tissues after oral dosing at 1.5 mg/kg body weight (Figs 2a and 2b). Free 4'-FIU reached a maximal plasma exposure of approximately 1 μM 90 minutes after oral administration, far exceeding the cell culture EC_{90} concentration against the influenza virus test panel. Plasma levels were sustained high over a 12-hour period after dosing. Corresponding 4'-FIU-TP tissue exposure levels 12 hours after dosing were approximately 1 nmol/g tissue in all organs but brain and kidney, underscoring suitability of 4'-FIU for *in vivo* efficacy testing against IAV.

Late-onset treatment with 4'-FIU mediates complete survival of IAV-infected animals

For mouse efficacy studies, animals were infected intranasally with a lethal inoculum amount of pandemic Ca09, which replicates efficiently in mice without a requirement for species adaptation [27].

Infection results in severe viral pneumonia with major clinical signs such as weight loss and hypothermia. To establish the lowest efficacious dose, we examined 3 4'-FIU dose levels in a survival study, each administered by oral gavage on three consecutive days in a once daily (q.d.) regimen starting at the time of infection (Fig 2c). All animals treated at the 2 mg/kg dose level survived, whereas all mice of the vehicle-treated and lowest dose (0.08 mg/kg) groups succumbed to infection within 5 days of inoculation (Fig 2d) and experienced clinical signs (S3a and S3b Figs). Animals receiving the intermediate 4'-FIU dose (0.4 mg/kg) had prolonged survival, but ultimately all died.

Having established 2 mg/kg 4'-FIU administered q.d. as a low efficacious dose, we next determined the latest time for initiation of effective treatment at this dose level (Fig 2e). All vehicle-treated animals again succumbed to infection within 5 days of inoculation (Fig 2f). In contrast, treatment start at 2.5 days after infection, which corresponds to 0.5 days after the onset of major clinical signs (S3c and S3d Figs) ensured complete survival, and 80% of animals of a group receiving the first dose 3 days after infection survived, outlining a broad therapeutic time window for treatment of influenza with 4'-FIU. Therapeutic benefit of late-onset treatment was corroborated by a significant reduction in lung virus load compared to vehicle-treated controls at 4.5 days after infection, determined in a parallel set of equally treated animals (Fig 2g). Within 7 days, virus became undetectable in lungs of animals that were treated starting 24 hours after infection with oral 4'-FIU (2 mg/kg q.d.; 3 doses total), indicating that viral replication had ceased (Fig 2h). No rebound of virus replication was observed within a 9-day period after infection (S3e and S3f Figs). These results define a broad therapeutic time window for effective treatment of IAV infection with 4'-FIU.

To determine the minimal number of oral 4'-FIU doses (2 mg/kg q.d.) for complete survival, we again initiated treatment 24 hours after infection, in this study comparing the effect of a single vs double or triple doses (Fig 2i). Lung virus load was assessed 4.5 days after infection and survival monitored in a parallel set of equally treated animals. The number of doses administered correlated with antiviral effect size, but even a single dose of 4'-FIU resulted in a statistically significant reduction in lung virus load of approximately one order of magnitude (Fig 2j). Reduced viral burden translated to survival of

some animals in the single and double dose groups. However, three doses were required for full therapeutic benefit (Fig 2k) and only mild clinical signs (S3g and S3h Figs).

4'-FIU effect on IAV transmission in the ferret model

Since mice, in contrast to ferrets, do not shed IAVs, we next explored anti-IAV efficacy of 4'-FIU in the ferret model. Guided by the dosing regimen established in mice, we treated animals infected intranasally with Ca09 with either 2 mg/kg (standard dose) or 0.5 mg/kg (low dose), administered orally starting 24 hours after infection (Fig 3a). Animals received one (2 mg/kg level) or two doses (either 2 or 0.5 mg/kg level) total. Fever is the predominant clinical sign associated with Ca09 IAV infection in ferrets. Monitoring body temperature continuously telemetrically, we observed significant reduction in all treated animals within 24 hours of the first dose, whereas vehicle-treated animals showed a prolonged fever plateau (S4a Fig). Viral titers in nasal lavages were statistically significantly reduced compared to those of vehicle animals, but effect size was lower in animals of the low dose than the standard dose group, and virus rebounded 2.5 days after infection in the single standard dose group (Fig 3b). In contrast, two standard doses 4'-FIU given q.d. were sterilizing within 2 days of treatment initiation. Virus load in nasal turbinates assessed 4 days after infection corroborated the lavage titers, revealing a dose-dependent significant antiviral effect of two doses, whereas a single dose had no significant effect on virus titer in turbinates at the time of tissue harvest (Fig 3c). Examination of lower respiratory tract tissues, trachea, and bronchoalveolar lavage fluid (BALF) revealed, however, that a single standard dose of 4'-FIU administered at the time of onset of clinical signs completely suppressed the development of viral pneumonia (Fig 3d).

To determine the effect of 4'-FIU on virus spread, we treated in a direct-contact transmission study source ferrets infected with Ca09 with the compound as before, starting 12 or 24 hours after infection (Fig 3e). Co-housing of source ferrets with untreated sentinels in a 1:1 ratio was initiated 2.5 days after study start. Ca09 rapidly spread from vehicle-treated source ferrets to their direct contacts, which first became virus-positive in nasal lavages only 12 hours after the beginning of co-housing (Fig 3f) and had progressed to viral pneumonia with high turbinate, lung and trachea virus load by study end (Fig 3g and 3h) and clinical signs (S4b and S4e Figs). Treatment of source animals with 4'-FIU initiated 12 or 24

hours after infection in each case resulted in exponential decline in shed virus load, but virus was undetectable in lavages of the 12-hour treatment group by the time of co-housing whereas approximately 10^4 $TCID_{50}$ units/ml lavage remained detectable in lavages of the 24-hour treatment group at that time. We did not detect any virus transmission to untreated sentinels of the 12-hour group. However, low-grade transmission to direct contacts of the 24-hour treatment group occurred, characterized by delayed onset of virus shedding compared to sentinels of vehicle-treated source animals and a reduced peak shed virus load (Fig 3h). Shedding from all sentinels that became virus-positive ceased approximately 12 days after the beginning of co-housing. These results confirm cross-species anti-IAV efficacy of 4'-FIU, reveal that a single oral dose is sufficient to prevent advance to severe influenza, and demonstrate a shortened window in which a treated case remains fully infectious.

Mitigation of IAV pathogenesis and lung histopathology by 4'-FIU

To better understand the impact of 4'-FIU on mitigating immunopathogenesis, the major driver of clinical signs associated with influenza virus infection, we determined inflammatory cytokine profiles for a 10-day period after infection of mice with Ca09 using a 6-plex Th17 cytokine assay (Fig 4a). Treated animals received the 3-dose standard 4'-FIU regimen as before, started 24 hours after infection. Lung tissue for histopathology was extracted from parallel sets of equally treated animals 5 or 21 days after infection. Lung titers in vehicle-treated animals demonstrated fast-onset viral pneumonia, approaching a burden of 10^6 infectious units/g lung tissue 4 days after infection, when all animals of the vehicle group had succumbed to infection with major clinical signs (Fig 4b, S5a and S5b Figs). Pro-inflammatory cytokines rapidly increased in the BALF of these animals, revealing a very strong antiviral response until death of the vehicle animals as expected after infection with Ca09 (Figs 4c and 4d, S6 Fig). Treatment with 4'-FIU again efficiently suppressed virus replication within 24 hours of the first dose (Fig 4b). Coinciding with the reduction in virus burden of treated animals by approximately two orders of magnitude by day 3 after infection, the proinflammatory response was greatly alleviated (Figs 4c and 4d, S6 Fig) and all treated animals survived (S5a Fig).

Consistent with a better clinical outcome (S7a and S7b Figs), lowered viral load, and mitigated innate antiviral response in 4'-FIU treated vehicle animals, analysis of lung histopathology 5 days after

infection revealed reduced lung lesions and alleviated cellular infiltrates in lung tissue of treated animals (Fig 4e, S8 Fig). Overall combined histopathology scores of individual animals representing the degree of cellular infiltrates into alveoli and bronchioles, the extent of perivascular cuffing, and the severity of interstitial pneumonia, pleuritis, and vasculitis were statistically significantly lower in the treatment than vehicle group (Fig 4f, S9 Fig).

4'-FIU control of influenza in immunocompromised hosts and of HPAI infection

In the clinic, the risk of progression to severe disease and poor overall outcome is greatly increased when immunocompetence of the patient is impaired or after zoonotic spillover of HPAIs into the human population [28, 29]. To first assess the potential of 4'-FIU to pharmacologically manage influenza in high-risk hosts, we infected interferon α/β receptor knockout (IFNAR1 KO) and V(D)J recombination activation gene RAG-1 KO mice with Ca09. Whereas the former cannot mount an effective type I IFN innate response [30, 31], the latter are compromised in their cell-mediated adaptive immunity due to a lack of mature T and B cells [32]. Oral treatment with 4'-FIU was initiated 24 hours after infection at standard and a high-dose (10 mg/kg) level, then continued q.d. for a total of 7 doses of each group (Fig 5a). Independent of 4'-FIU dose level, all treated animals of the RAG-1 KO and IFNAR1 KO groups survived, whereas all animals in the vehicle-treated groups developed severe clinical signs (S10a to S10d Figs) and succumbed to infection within 4 days (Fig 5b). Reduction in lung virus load of treated vs vehicle animals after three q.d. 4'-FIU doses (day 4 after infection) was dose level-dependent, but even at the standard dose, this reduction exceeded two orders of magnitude in either knockout mouse strain (Fig 5c).

Next, we explored 4'-FIU efficacy against HPAIs, initially testing potency against polymerases derived from A/CA/07/2009 (H1N1), A/VN/12/2003 (H5N1), and A/Anhui/1/2013 (H7N9) in minireplicon dose-response assays (Fig 5d). The compound dose-dependently inhibited activity of either HPAI-derived polymerase complex, reaching active concentrations resembling that observed against Ca09 RdRP. Selecting A/VN/12/2003 (H5N1), which causes lethal encephalitis in mice [33], for a proof-of-concept efficacy study of 4'-FIU against zoonotic HPAIs, we started treatment at the 5 mg/kg dose level 12 or 24 hours after infection and continued q.d. thereafter (Fig 5e). None of the animals of either 4'-FIU

treatment group developed clinical signs even when treatment was initiated 24 hours after infection (Fig 5f), and all treated animals survived (Fig 5g). In contrast, all vehicle-treated animals succumbed to A/VN/12/2003 (H5N1) with a median survival time of 9 days after infection, developing clinical signs on day 7 after infection followed by rapid further deterioration (Fig 5f). Vehicle-treated animals experienced high lung virus loads three days after infection (Fig 5h). Treatment reduced HPAI burden by several orders of magnitude to limit of detection. These results confirm uncompromised efficacy of 4'-FIU in high-risk immunocompromised hosts and against highly pathogenic zoonotic viruses with high pandemic concern.

Anti-IAV immune status of 4'-FIU-treated recoveries

Highly efficacious antivirals may suppress host immune activation, especially when treatment is started early in the course of infection, which may leave the host susceptible to subsequent re-infection and may potentially even result in exacerbated disease [34-36]. To explore the effect of 4'-FIU on subsequent homotypic IAV rechallenge of recoveries, we infected animals with Ca09 and started standard 3-dose 4'-FIU treatment at three time points, therapeutically at 24 and 48 hours after infection and prophylactically at 12 hours before infection (Fig 6a). For this study, mice were inoculated with aerosolized virus in a temperature and airflow-controlled aerosol chamber using an Aeroneb nebulizer (S11a and S11b Figs) to better mimic natural infection. Prior to study start, we performed pilot experiments to determine suitable exposure time (S12a to S12c Figs), infectious dose (S13a and S13b Figs) and proof-of-concept for 4'-FIU efficacy (S14a to S14d Figs) after infection with aerosolized virus. Mirroring the outcome of our previous efficacy studies, animals of all treatment groups survived the original infection, whereas all animals of the vehicle group reached predefined clinical endpoints 9 days after infection and had to be terminated (Fig 6b) with major clinical signs (S15a and S15b Figs). To assess the status of humoral anti-Ca09 immunity, we collected blood samples from the treated recoverees 4, 8, and 12 weeks after the original infection and determined neutralizing antibody (nAb) titers. Mice in both therapeutic treatment groups mounted a robust humoral anti-IAV response, whereas no nAbs were detectable in the prophylactically treated animals 8 weeks after the original infection (Fig 6c). Upon homotypic rechallenge with aerosolized Ca09 10 weeks after the original infection, however,

all 4'-FIU-experienced recoverees had a significant benefit over a new set of IAV-naïve mice (Fig 6d). All animals of the therapeutic groups survived with significant boost in nAb titers relative to week 8 levels. Remarkably, four of the five animals treated prophylactically with 4'-FIU at the time of the original infection also survived the homotypic rechallenge and mounted a robust humoral anti-Ca09 response by week 12. In contrast, all newly added IAV-inexperienced animals succumbed to infection within 9 days, confirming efficient virus delivery through aerosolization at rechallenge. Animals of the treatment group remained disease-free during rechallenge, and clinical signs were alleviated in mice of the prophylactic group (S15c and S15d Figs). Independent of the original 4'-FIU regimen applied, we did not detect any signs of exacerbated disease upon rechallenge of treatment-experienced recoverees.

Discussion

Treatment of influenza has remained challenging, despite the current availability of two different FDA-approved drug classes, the neuraminidase and endonuclease inhibitors [37]. The main challenges to more successful antiviral therapies are narrow therapeutic time windows [38], poor patient compliance [39], and impaired immunocompetence of older adults at greatest risk of advance to severe disease [17], defining key developmental objectives for the next generation of influenza therapeutics.

Demonstrating antiviral potency in cell culture, human airway organoids, and/or efficacy in two relevant *in vivo* infection models, ferrets and mice, this study establishes oral efficacy of 4'-FIU, a broad-spectrum antiviral ribonucleoside analog [24, 25], against seasonal, pandemic, and HPAI IAV strains. Designed to expand our first-line pharmacological arsenal against RNA viruses of pandemic concern, we have previously shown activity of 4'-FIU against SARS-CoV-2, pneumoviruses such as RSV and paramyxoviruses [24]. Mechanistic characterization consistently demonstrated that incorporation of 4'-FIU-TP into the nascent RNA strand induces polymerase chain termination [24]. Unique to 4'-FIU of all chain-terminating ribonucleoside analogs analyzed [25], however, the modus of 4'-FIU-induced termination varies dependent on RdRP target. IAV RdRP stalled immediately upon incorporation, RSV polymerase termination was delayed at position *i*+3 after incorporation, and SARS-CoV-2 polymerase termination was delayed and dependent on sequence context, requiring

296 incorporation of at least two 4'-FIU moieties in close repetition [24]. Delayed chain termination typically
297 reflects that incorporation of the nucleoside analog alters secondary structure of the nascent strand,
298 which interferes with polymerase processivity [25, 40, 41]. Accordingly, we hypothesize that distinct
299 mechanisms of action (MOAs) against betacoronaviruses, pneumoviruses, and orthomyxoviruses are
300 due to different capabilities of the respective polymerase complexes to accommodate 4'-FIU-specific
301 secondary structure changes.

302 In clinical trials of baloxavir marboxil, viral resistance emerged rapidly, resulting in rebound of virus
303 replication in 82.1% of treated patients [23]. Whole genome sequencing of 4'-FIU-experienced virus
304 populations isolated from infected and treated animals showed no allele-dominant divergence from the
305 inoculum population, suggesting a high genetic barrier against resistance to 4'-FIU [24]. It will
306 nevertheless be exciting to explore whether future resistance profiling of the compound against different
307 viral targets, including IAV, RSV, and SARS-CoV-2, is feasible and may illuminate residues that control
308 structural flexibility of the polymerase complexes rather than substrate specificity.

309 Very likely representing a direct consequence of the distinct MOAs, however, we found influenza
310 viruses to be most sensitive to inhibition by 4'-FIU, followed by RSV and SARS-CoV-2. Dose-finding in
311 the mouse model identified effective levels in the low mg/kg range and three doses administered q.d. to
312 be sufficient for achieving full therapeutic benefit, which resembled efficacy performance of baloxavir
313 marboxil [42] and far outpaced that of the neuraminidase inhibitors [43]. Whereas therapeutic
314 oseltamivir lacked efficacy in mice infected with pdm09 IAV isolates [44] and baloxavir marboxil
315 ensured only partial survival when treatment was started later than 24 hours after infection [42],
316 treatment with 4'-FIU mediated unprecedented complete survival of all treated animals when the
317 inhibitor was first administered as late as 60 hours after infection, at the time when lung virus burden
318 approached peak titer [45] and major clinical signs had manifested. If predictive of the treatment of
319 human disease, this substantially widened therapeutic time window may be game-changing for
320 influenza therapy.

321 Since clinical signs of influenza are largely a result of immunopathogenesis [46], we asked whether
322 4'-FIU may impact the quality of the antiviral immune response and potentially trigger exacerbated

disease upon homotypic re-infection. Cytokine profiling showed an alleviated pro-inflammatory response in animals dosed therapeutically with 4'-FIU, but assessment of neutralizing antibody titers revealed that each of the treated animals had mounted a robust humoral response. Consistent with our previous observation of low cytotoxic and cytostatic potential of 4'-FIU [24], these results indicate that mitigated immunopathogenesis in treated animals is a consequence of reduced virus load rather than a direct immunomodulatory effect of the compound. Although essentially sterilizing, even prophylactic treatment resulted in partial protection of animals at re-infection despite the absence of neutralizing antibodies, indicating that treated animals also mounted a viable cell-mediated adaptive response [47, 48].

Beyond individual patient benefit through mitigation of lethal infection and alleviation of viral pneumonia and lung immunopathogenesis, 4'-FIU statistically significant reduced upper respiratory tract virus load and viral shedding when treating 12 hours after infection, resulting in fully suppressed spread to untreated direct-contact sentinels in the highly sensitive ferret transmission model [49]. Later treatment initiation still reduced transmission efficiency, resulting in delayed onset of virus replication and reduced upper respiratory tract peak virus load, which serves as a biomarker for risk of progression to severe viral pneumonia [50]. If equally applicable to the human host, pharmacological block or mitigation of transmission provides a promising path towards outbreak control through efficient interruption of community transmission chains, mitigating the health threat and economic burden [51] of endemic and pandemic influenza.

At greatest risk of life-threatening disease are the immunocompromised [52, 53] and patients infected with zoonotic HPAI viruses [54, 55]. When assessed in an immunocompromised mouse model, baloxavir marboxil returned a significantly prolonged time to death, but ultimately all animals succumbed to the infection [56]. In contrast, treatment with 4'-FIU mediated complete survival of all animals in two distinct immunocompromised mouse models, underscoring powerful antiviral activity that does not strictly depend on a fully immunocompetent host to clear the infection [57]. Adding efficient control of highly pathogenic zoonotic IAVs, we propose that 4'-FIU meets key efficacy requirements of a next-generation antiviral clinical candidate that strengthens pandemic preparedness and provides a

much-needed alternative option for management of seasonal and pandemic influenza viruses.

Material and Methods

Study design

Cells, ferrets and mice were used as *in vitro*, *ex vivo* and *in vivo* models, respectively, to examine efficacy of 4'-FIU against Influenza infections. Biochemical RdRP assays were added for mechanistic characterization against the influenza virus target. Viruses were administered through intranasal or aerosolized (mice only) inoculation and virus load monitored periodically in nasal lavages (ferrets only), and in respiratory tissues of ferrets and mice extracted 4 days and 3-14 days, respectively, after infection. Virus titers were determined through $TCID_{50}$-titration.

Cells, viruses, and compound synthesis

MDCK (ATCC CCL-34) and 293T (ATCC CRL-3216) cells were cultured in Dulbecco's modified Eagle's medium (DMEM) supplemented with 7.5% heat-inactivated fetal bovine serum (FBS) at 37°C and 5% CO_2. Human primary cells were grown in epithelial differentiation medium [24]. A/duck/Alberta/35/76 (H1N1), A/swine/Spain/53207/2004 (H1N1), A/Wisconsin/67/2005 (H3N2), A/California/07/2009 (H1N1)pdm09, A/Netherlands/602/2009 (H1N1)pdm09, A/WSN/33 (H1N1), and A/Wyoming/03/2003 (H3N2), as well as B/Brisbane/60/08 were propagated on MDCK cells using serum-free DMEM supplemented with 0.5% Trypsin. A/Viet Nam/1203/2004 (H5N1) was propagated in the allantoic cavity of embryonated hen eggs at 37°C for 24 hours, clarified, aliquoted, and stored at −80°C. The titer of A/Viet Nam/1203/2004 (H5N1) was determined by plaque assay on MCDK cells. Virus stock titers were determined through $TCID_{50}$-titration, stocks were stored in aliquots at -80°C. Recombinant influenza viruses were recovered using an 8-plasmid system generated for A/CA/07/2009 (H1N1) that was based on original reports for laboratory-adapted IAV [58]. Reporter viruses were generated through insertion of a nanoLuc or maxGFP-encoding ORF in frame at the 5'-end of the viral HA ORF, separated by a 2A cleavage site as described for other recombinant IAVs [59]. Genetic stability of the resulting nanoLuc-HA and maxGFP-HA segments was validated through sequence confirmation after 10 consecutive viral passages on MDCK cells. 4'-FIU was synthesized from 5'-(3-

chlorobenzoyloxy)-2',3'-di-O-acetyl-4'-fluorouridine and 4N ammonia in methanol as previously described [24], authenticated through elemental analysis, and stored as dry powder. Working aliquots were dissolved in DMSO or 10% methylcellulose for *in vitro* and *in vivo* studies, respectively.

Primary human airway epithelium organoid cultures

Primary HAEs (3×10^5/well) at passage <3 were seeded on 6.5 mm 0.4 μm pore size polyester inserts (Corning Costar Transwell) and differentiated for at least 21 days at air-liquid interface using Air-Liquid Interface Differentiation Medium (LifeLine Cell Technology). Transepithelial/transendothelial resistance (TEER) was monitored using an EVOM volt/ohm meter coupled with STX2 electrode (World Precision Instruments). Developing organoids were washed apically at least once per week to remove mucus. For infection virus was added apically, treatment occurred through compound addition to the basolateral chamber.

Virus titration

Virus samples were serially diluted (10-fold starting at 1:10 initial dilution) in serum-free DMEM supplemented with 0.5% Trypsin (Gibco). Serial dilutions were added to MDCK cells seeded in 96-well plate at 1×10^4 cells per well 24 hours before infection. Infected plates were incubated for 72 hours at 37°C with 5% CO_2, followed by transfer of culture supernatants to suspension of chicken red blood cells and scoring of wells based on hemagglutination activity. A/Viet Nam/1203/2004 (H5N1) virus and samples were titered by plaque assay; serially diluted 10-fold in DMEM with 2% FBS, added to MDCK cells in 12-well plates and overlaid with DMEM+2% FBS with 1.2% Avicel microcrystalline cellulose. Plates were incubated for 48 hours at 37°C with 5% CO_2, then washed, fixed with methanol:acetone (80:20), and counter-stained with crystal violet to visualize plaques.

Minigenome assay

293T cells were seeded and transfected with 1.0 μg of luciferase-encoding reporter plasmid [26] and 0.5 μg each of PB1, PB2, NP and PA expression plasmids derived from A/California/07/2009 (H1N1), A/Viet Nam/1203/2004 (H5N1), and A/Anhui/1/2013 (H7N9), respectively. Three hours post transfection, 4'-FIU or vehicle (DMSO) volume equivalents were added in 3-fold serial dilution series starting at 20 μM 4'-FIU concentration, followed by incubation for 30 hours at 37°C and determination of

luciferase activity using a BioTek Synergy H1 multimode plate reader. Relative activities were calculated according to the formula % relative activity = $(RLU_i - RLU_{min})/(RLU_{max} - RLU_{min}) \times 100$, with RLU_i specifying sample luciferase value, RLU_{min} specifying values from equally transfected, vehicle-treated cells that did not receive the PB2 subunit encoding plasmid, and RLU_{max} specifying values from fully transfected, vehicle-treated cells.

Dose-response assays

Active concentrations (EC_{50} and EC_{90}) of 4'-FlU were calculated through 4-parameter variable slope regression modeling of dose-response assay data, derived from minigenome assays, luciferase reporter virus assays, or progeny virus yield ($TCID_{50}$) assays as specified. Test article was in all cases assessed in 3-fold serial dilutions.

Recombinant IAV RdRP expression and purification

A/CA/07/2009 (H1N1)-derived PA, PB1, and PB2 expression plasmids were subcloned into the pFastbac Dual plasmid expression vector (Invitrogen) with polyhedrin promoter control. An TEV protease-cleavable N-terminal hexahistidine-tag was added to the PA subunit to facilitate purification of the complex through affinity chromatography. The individual plasmids were transformed in DH10bac cells and the resulting bacmid transfected into SF9 cells. After virus recovery, SF9 cells were infected with the three individual viruses in the ratio of 1:1:2. Cells were harvested after 72 hours and lysed in lysis buffer (Tris 50 mM pH 7.4, NaCl 300 mM, NP 40 0.5%, protease inhibitor cocktail, glycerol 10%, TCEP 0.5 mM) on ice for two hours, followed by sonication. Clarified supernatant was incubated at 4°C for 1 hour with Ni-NTA beads which were pre-equilibrated with Tris 50 mM pH 7.4, NaCl 300 mM, NP 40 0.2%, glycerol 10%, TCEP 0.5 mM containing 20 mM imidazole. After extensive washing with Tris 50 mM pH 7.4, NaCl 300 mM, NP 40 0.2%, glycerol 10%, TCEP 0.5 mM containing 20-50 mM imidazole, protein complexes were eluted in buffer Tris 50 mM pH 7.4, NaCl 300 mM, NP 40 0.2%, glycerol 10%, TCEP 0.5 mM containing 250 mM imidazole. Eluted protein fractions were pooled and loaded on heparin HP columns, which were flushed with buffer A (Tris 50 mM pH 7.4, NaCl 250 mM, glycerol 10%), then 0-100% of buffer B (Tris 50 mM pH 7.4, NaCl 1M, glycerol 10%) diluted in buffer A. The polymerase complex peak was observed in ~80% buffer B, which corresponds to approximately

900 mM NaCl in the buffer. Peak fractions were collected separately and dialyzed against buffer C (Tris/Cl 50 mM pH 7.4, NaCl 150 mM, glycerol 10%) in dialyzing cassettes at 4°C overnight. Purified protein complexes were harvested, aliquoted and stored at -80°C until use.

In vitro RdRP primer extension assay

In vitro primer extension assays were carried out essentially as described [24, 60]. Briefly, RdRP assay reactions were set up in 20 mM Tris-HCl pH 7.4, 10% glycerol, 1 mM TCEP, 3 mM MnCl2, 2 µM RNA template, 100 µM RNA primer, and nucleotides and 1 µCi of α^{32}P-labelled ATP (Perkin-Elmer) as specified in the figure legends, followed by incubation at 30°C for 10 minutes. Polymerase complexes were added to the reaction and incubation continued for 1 hour at 30°C. Reactions were stopped with 1 volume of deionized formamide containing 25 mM ethylenediaminetetraacetic acid (EDTA), followed by a denaturation step at 95°C. Amplicons were fractionated on 20% polyacrylamide gels with 7M urea, using a Tris-Borate-EDTA electrophoresis buffer. Amplicons were visualized by autoradiography, using a storage phosphor screen BAS IP MS 2040 E (GE Healthcare Life Sciences) and Typhoon FLA 7000 (GE Healthcare Life Sciences) imager. Densitometry analysis was performed using FIJI 2.1.0. To determine enzyme kinetics (V_{max} and K_m), Michaelis-Menten equation was applied in Prism 9.0.0 (GraphPad).

Pharmacokinetic property and tissue distribution profiling in mice

Male and female C57BL/6J mice were rested for 3 days prior to study start. Then, animals were gavaged with 1.5 mg/kg bodyweight 4'-FIU in 10 mM sodium citrate with 0.5% Tween 80, final gavage volume 200 µl. Blood samples (150 µl) were taken at 90 minutes, 3 hours and 12 hours after dosing, cleared (2,000 rpm, 5 minutes, 4°C), and extracted plasma stored at -80°C. Organ samples (lung, brain, spleen, heart, kidney and liver) were harvested 12 hours after dosing and snap-frozen in liquid nitrogen. Animal tissues were homogenized with 70% acetonitrile in water that included internal standards. Animal plasma and tissue concentrations of 4'FIU and 4'-FIU-TP were measured by a qualified LC/MS/MS method in MRM mode on a QTRAP 5500 (Sciex, Santa Clara, CA, USA) instrument.

Intranasal infection of mice

Female or male mice (5-8 weeks of age, Balb/c, RAG1 KO or IFNar KO) were purchased from Jackson Laboratories. Upon arrival, mice were rested for at least 3 days, then randomly assigned to study groups and housed under ABSL-2 or ABSL-3 conditions for infections with A/CA/07/2009 (H1N1) recombinants or A/VN12/2003 (H5N1), respectively. Bodyweight was determined twice daily, body temperature determined once daily rectally. For infections, animals were anesthetized with isoflurane or isoflurane/ketamine (H5N1 challenge only), followed by intranasal inoculation with 2.5×10^{1} $TCID_{50}$ units/animal of A/CA/07/2009 (H1N1), 1×10^{3}- 1×10^{5} $TCID_{50}$ units/animal of GFP or nanoLuc expressing reporter virus versions of A/CA/07/2009 (H1N1), or 6×10^{1} of A/VN12/2003 (H5N1). In all cases, virus inoculum was diluted in 50 µl and administered in amounts of 25 µl per nare. Animals were euthanized and organs harvested at predefined time points or when animals reached humane study endpoints.

4'-FIU anti-IAV efficacy studies in mice

Mice were inoculated intranasally with IAV stocks as described, followed by treatment with 4'-FIU at specified dose levels and starting time points through oral gavage. Unless specified otherwise, treatment was continued q.d. Each individual study contained animals receiving equal volumes of vehicle through oral gavage. At study end point, lung tissue was harvested for virus titration or histopathology assessment. For tissue fixation, lungs were perfused using 10% neutral-buffered formalin [10% formalin, NaH_2PO_4 (4 g/liter), and Na_2HPO_4 (6.5 g/liter)], dissected, and fixed for 24 hours. Formalin-fixed lungs were transferred to 70% EtOH after 72 hours, embedded in paraffin, sectioned (5-µm thickness), and stained with hematoxylin and eosin. Slides were evaluated by a licensed pathologist. A pathology score range of 0 to 3 was used to evaluate tissue damage. For analysis of proinflammatory cytokine levels through Bioplex, lungs of euthanized mice were lavaged with 1 ml sterile PBS to extract BALFs, and cleared BALF analyzed against the Standard Th17-panel (Bio-Rad) according to the manufacturer's instructions.

Efficacy studies in ferrets

Female ferrets (6-10 months of age) were purchased from Triple F Farms. Upon arrival, ferrets were rested for 1 week, then randomly assigned to study groups and housed in groups of three animals under ABSL-2 conditions. In some studies, animals received a temperature sensor for continued

telemetric measurement of body temperature. Otherwise, body temperature was determined rectally once daily. Dexmedetomidine/ketamine anesthetized animals were inoculated intranasally with 1×10^5 $TCID_{50}$ units of A/CA/07/2009 (H1N1) in a volume of 300 µl per nare. Nasal lavages were performed twice daily using 1 ml of PBS containing 2× antibiotics-antimycotics (Gibco). Treatment with 4'-FIU through oral gavage followed a q.d. regimen. Ferrets were terminated four days post infection and BALF and organ (lungs, turbinates and tracheas) samples extracted for virus titrations.

Ferret transmission studies

Female ferrets (3-8 months of age) were anesthetized with dexmedetomidine/ketamine and infected intranasally with 1×10^5 $TCID_{50}$ units of A/CA/07/2009 (H1N1) as before. Nasal lavages were performed every 12 hours, bodyweight and temperature determined once daily. Treatment of source animals was initiated 12 or 24 hours after infection at a dose of 2mg/kg bodyweight, and continued q.d. for three doses total. Starting day 2.5 after infection, uninfected and untreated contact animals were added to the infected and treated source ferrets to allow direct-contact transmission, and co-housing continued until termination of the source ferrets on study day 4. Sentinels were subjected to once daily nasal lavages and monitored until study day 10 or, when infectious particles were detected in lavages of contacts of 4'-FIU-treated source animals, study day 14.

Virus titration from tissue samples

Organs were weighed and homogenized in 500 µl PBS using a beat blaster, set to 3 cycles of 30 seconds each at 4°C, separated by 1-minute rest periods. Homogenates were cleared (10 minutes at 20,000 × g and 4°C), and cleared supernatants stored at -80°C until virus titration. Viral titers were expressed as $TCID_{50}$ units per gram input tissue. For A/VN12/2003 (H5N1), lungs were homogenized using a TissueLyzer (Qiagen), clarified by centrifugation, supernatants aliquoted, and then stored at -80°C. A/VN12/2003 (H5N1) virus titer was determined by plaque assay and expressed as PFU per ml of lung homogenate.

Infection of mice with aerosolized A/CA/07/2009 (H1N1)

An Aeroneb (Kent Scientific) system was used to infect mice (female Balb/c, 6-8 weeks of age) with aerosolized IAV. Conscious animals were transferred to an aerosol chamber placed on a heat pad

adjusted to 37°C to prevent condensation, connected to the nebulizer unit (Aeroneb with palladium mesh) and air pump with airflow restrictor. For condition-finding experiments, the nebulizer chamber was loaded with virus inoculum diluted to 1×10^3-1×10^5 $TCID_{50}$ A/CA/07/2009 (H1N1) per ml in sterile PBS, airflow adjusted to 1 l/minute, and animals continuously exposed for 3, 10, or 30 minutes. For treatment studies, conditions were adjusted to 1×10^5 $TCID_{50}$/ml in sterile PBS, 10 minutes exposure time, and 1 l/minute airflow.

Re-infection of 4'-FIU-experienced mice with A/CA/07/2009 (H1N1)

Mice infected with aerosolized A/CA/07/2009 (H1N1) as above were treated q.d. with 4'-FIU or vehicle as specified, and monitored for 10 weeks or until humane endpoints were reached. Blood was collected 4 and 8 weeks after infection and A/CA/07/2009 (H1N1)-neutralizing antibody titers determined. Treated recoverees were reinfected with homotypic, aerosolized A/CA/07/2009 (H1N1) 10 weeks after the original infection along with a fresh set of naïve animals, followed by monitoring for an additional 14 days and final blood collection at study end. No treatment was administered after reinfection.

Neutralizing antibody titers in mice

Plasma was prepared from blood samples (2,000 rpm, 10 minutes, 4°C and stored at -80°C until analysis. Heat-inactivated plasma was incubated with 100 $TCID_{50}$ units of A/CA/07/2009 (H1N1) (H1N1) for 90 minutes, followed by serial dilution and transfer to MDCK cells, and plates incubated for 3 days at 37°C. Remaining infectivity was visualized through hemagglutination activity on chicken red blood cells.

Statistical analysis

For statistical analysis of studies consisting of only two groups, unpaired two-tailed t-tests were applied. When comparing more than two study groups, 1-way analysis of variance (ANOVA) or 2-way ANOVA with multiple comparison *post hoc* tests as specified were used to assess statistical difference between samples. Statistical analyses were carried out in Prism version 9.4.1 (GraphPad). The number of individual biological replicates (n values) and exact P values are shown in the figures when possible. The threshold of statistical significance (α) was set to 0.05. Source data and statistical analysis are

shown in S1 and S2 Data files, respectively.

Ethical compliance

All animal work was performed in compliance with the *Guide for the Care and Use of Laboratory Animals* of the National Institutes of Health and the Animal Welfare Act Code of Federal Regulations. Experiments involving mice and ferrets were approved by the Georgia State University Institutional Animal Care and Use Committee (IACUC) under protocols A20012 and A21020, respectively. *In vivo* experimentation with HPAI viruses was approved by the University of Georgia at Athens IACUC under protocol A2020 03-033. All experiments using infectious material were approved by the Georgia State University and the University of Georgia at Athens Institutional Biosafety Committees (IBCs) and performed in BSL-2/ABSL-2 or BSL-3/ABSL-3 containment facilities, respectively. Experiments involving HPAI were reviewed and approved by the IBC of the University of Georgia at Athens and were conducted in enhanced biosafety level 3 (BSL3+) containment according to guidelines for the use of select agents approved by the CDC.

Acknowledgements

We thank AC Lowen for IAV and IBV virus isolates and the Georgia State University Department of Animal Resources for Assistance.

Competing Interests

MGN and GRP are coinventors on patent WO 2019/1736002 covering composition of matter and use of 4'-FIU (EIDD-2749) and its analogs as an antiviral treatment. This study could affect their personal financial status. RKP reports contract testing from Enanta Pharmaceuticals and Atea Pharmaceuticals, and research support from Gilead Sciences, outside of the described work. All other authors declare that they have no competing interests.

References

1. Greenwood M. The Epidemiology of Influenza. Br Med J. 1918;2(3021):563-6. Epub 1918/11/23. doi: 10.1136/bmj.2.3021.563. PubMed PMID: 20769264; PubMed Central PMCID: PMCPMC2342100.

2. Sendor AB, Weerasuriya D, Sapra A. Avian Influenza. StatPearls. Treasure Island (FL): StatPearls Publishing Copyright © 2022, StatPearls Publishing LLC.; 2022.
3. Christie Wilcox TS. Unprecedented Avian Flu Epidemic Could Presage Year-Round Outbreaks 2022. Available from: https://www.the-scientist.com/news-opinion/unprecedented-avian-flu-epidemic-could-presage-year-round-outbreaks-70584?utm_campaign=TS_DAILY_NEWSLETTER_2022&utm_medium=email&_hsmi=228465931&_hsenc=p2ANqtz-8TgW7-yAeXmDwdZXM5FZG2PFR9rD1ZgiLLf7s9vbRNouK_QcXXckHpbv606nJ0vnXWU8KCDXHcq6xrTI8qoiSj6M0XPA&utm_content=228465931&utm_source=hs_email.
4. ECDC. 2021-2022 data show largest avian flu epidemic in Europe ever, last excessed 10/21/2022: European Centre for Disease Prevention and Control; 2022. Available from: https://www.ecdc.europa.eu/en/news-events/2021-2022-data-show-largest-avian-flu-epidemic-europe-ever.
5. Morens DM, Taubenberger JK. Pandemic influenza: certain uncertainties. Rev Med Virol. 2011;21(5):262-84. Epub 20110627. doi: 10.1002/rmv.689. PubMed PMID: 21706672; PubMed Central PMCID: PMCPMC3246071.
6. CDC. History of 1918 Flu Pandemic, last excessed 10/07/2022: Centers for Disease Control and Prevention; 2018. Available from: https://www.cdc.gov/flu/pandemic-resources/1918-commemoration/1918-pandemic-history.htm.
7. Taubenberger JK, Kash JC, Morens DM. The 1918 influenza pandemic: 100 years of questions answered and unanswered. Sci Transl Med. 2019;11(502). Epub 2019/07/26. doi: 10.1126/scitranslmed.aau5485. PubMed PMID: 31341062.
8. Cheung JTL, Lau EH, Jin Z, Zhu H, Guan Y, Peiris M. Influenza A virus transmission in swine farms and during transport in the swine supply chain. Transbound Emerg Dis. 2022;69(5):e3101-e10. Epub 2022/07/27. doi: 10.1111/tbed.14667. PubMed PMID: 35881331.
9. CDC. 2009 H1N1 Pandemic (H1N1pdm09 virus), last excessed 10/07/2022: Centers for Disease Control and Prevention; 2019. Available from: https://www.cdc.gov/flu/pandemic-resources/2009-h1n1-pandemic.html.
10. Yang JH, Huang PY, Shie SS, Yang S, Tsao KC, Wu TL, et al. Predictive Symptoms and Signs of Laboratory-confirmed Influenza: A Prospective Surveillance Study of Two Metropolitan Areas in Taiwan. Medicine (Baltimore). 2015;94(44):e1952. Epub 2015/11/12. doi: 10.1097/md.0000000000001952. PubMed PMID: 26554802; PubMed Central PMCID: PMCPMC4915903.
11. Florescu DF, Kalil AC. The complex link between influenza and severe sepsis. Virulence. 2014;5(1):137-42. Epub 2013/11/21. doi: 10.4161/viru.27103. PubMed PMID: 24253109; PubMed Central PMCID: PMCPMC3916367.
12. Kido H, Chida J, Yao M, Wang S. [Mechanisms of multi-organ failure in severe influenza]. Nihon Rinsho. 2010;68(8):1565-73. Epub 2010/08/19. PubMed PMID: 20715496.
13. Radovanovic M, Petrovic M, Barsoum MK, Nordstrom CW, Calvin AD, Dumic I, et al. Influenza Myopericarditis and Pericarditis: A Literature Review. J Clin Med. 2022;11(14). Epub 2022/07/28. doi: 10.3390/jcm11144123. PubMed PMID: 35887887; PubMed Central PMCID: PMCPMC9316162.
14. Vousden N, Knight M. Lessons learned from the A (H1N1) influenza pandemic. Best Pract Res Clin Obstet Gynaecol. 2021;76:41-52. Epub 2020/11/05. doi: 10.1016/j.bpobgyn.2020.08.006. PubMed PMID: 33144076; PubMed Central PMCID: PMCPMC7550184.
15. CDC. Vaccine Effectiveness: How Well Do Flu Vaccines Work?, last excessed 10/05/2022: Centers for Disease Control and Prevention; 2022. Available from: https://www.cdc.gov/flu/vaccines-work/vaccineeffect.htm.
16. Pleguezuelos O, James E, Fernandez A, Lopes V, Rosas LA, Cervantes-Medina A, et al. Efficacy of FLU-v, a broad-spectrum influenza vaccine, in a randomized phase IIb human influenza challenge study. NPJ Vaccines. 2020;5(1):22. Epub 2020/03/21. doi: 10.1038/s41541-020-0174-9. PubMed PMID: 32194999; PubMed Central PMCID: PMCPMC7069936.
17. CDC. Influenza Antiviral Medications: Summary for Clinicians, last excessed 10/05/2022: Centers for Disease Control and Prevention; 2022. Available from: https://www.cdc.gov/flu/professionals/antivirals/summary-clinicians.htm.

18. Nelson MI, Simonsen L, Viboud C, Miller MA, Holmes EC. The origin and global emergence of adamantane resistant A/H3N2 influenza viruses. Virology. 2009;388(2):270-8. Epub 2009/04/28. doi: 10.1016/j.virol.2009.03.026. PubMed PMID: 19394063; PubMed Central PMCID: PMCPMC2705899.
19. Hussain M, Galvin HD, Haw TY, Nutsford AN, Husain M. Drug resistance in influenza A virus: the epidemiology and management. Infect Drug Resist. 2017;10:121-34. Epub 2017/05/02. doi: 10.2147/idr.S105473. PubMed PMID: 28458567; PubMed Central PMCID: PMCPMC5404498.
20. CDC. Antiviral Drug Resistance among Influenza Viruses, last excessed 10/07/2022: Centers for Disease Control and Prevention; 2016. Available from: https://www.cdc.gov/flu/professionals/antivirals/antiviral-drug-resistance.htm.
21. Patel MC, Mishin VP, De La Cruz JA, Chesnokov A, Nguyen HT, Wilson MM, et al. Detection of baloxavir resistant influenza A viruses using next generation sequencing and pyrosequencing methods. Antiviral Res. 2020;182:104906. Epub 2020/08/18. doi: 10.1016/j.antiviral.2020.104906. PubMed PMID: 32798601; PubMed Central PMCID: PMCPMC7426223.
22. CDC. Influenza Antiviral Drug Baloxavir Marboxil, last excessed 10/03/2022: Centers for Disease Control and Prevention; 2022. Available from: https://www.cdc.gov/flu/treatment/baloxavir-marboxil.htm.
23. Ince WL, Smith FB, O'Rear JJ, Thomson M. Treatment-Emergent Influenza Virus Polymerase Acidic Substitutions Independent of Those at I38 Associated With Reduced Baloxavir Susceptibility and Virus Rebound in Trials of Baloxavir Marboxil. J Infect Dis. 2020;222(6):957-61. Epub 2020/04/08. doi: 10.1093/infdis/jiaa164. PubMed PMID: 32253432.
24. Sourimant J, Lieber CM, Aggarwal M, Cox RM, Wolf JD, Yoon JJ, et al. 4'-Fluorouridine is an oral antiviral that blocks respiratory syncytial virus and SARS-CoV-2 replication. Science. 2022;375(6577):161-7. Epub 2021/12/03. doi: 10.1126/science.abj5508. PubMed PMID: 34855509.
25. Lieber CM, Plemper RK. 4'-Fluorouridine Is a Broad-Spectrum Orally Available First-Line Antiviral That May Improve Pandemic Preparedness. DNA Cell Biol. 2022;41(8):699-704. Epub 20220705. doi: 10.1089/dna.2022.0312. PubMed PMID: 35788144; PubMed Central PMCID: PMCPMC9416544.
26. Yan D, Weisshaar M, Lamb K, Chung HK, Lin MZ, Plemper RK. Replication-Competent Influenza Virus and Respiratory Syncytial Virus Luciferase Reporter Strains Engineered for Co-Infections Identify Antiviral Compounds in Combination Screens. Biochemistry. 2015;54(36):5589-604. Epub 2015/08/27. doi: 10.1021/acs.biochem.5b00623. PubMed PMID: 26307636; PubMed Central PMCID: PMCPMC4719150.
27. Kiseleva I, Rekstin A, Al Farroukh M, Bazhenova E, Katelnikova A, Puchkova L, et al. Non-Mouse-Adapted H1N1pdm09 Virus as a Model for Influenza Research. Viruses. 2020;12(6). Epub 2020/06/04. doi: 10.3390/v12060590. PubMed PMID: 32485821; PubMed Central PMCID: PMCPMC7354452.
28. Hayden FG. Prevention and treatment of influenza in immunocompromised patients. Am J Med. 1997;102(3A):55-60; discussion 75-6. Epub 1997/03/17. PubMed PMID: 10868144.
29. Kunisaki KM, Janoff EN. Influenza in immunosuppressed populations: a review of infection frequency, morbidity, mortality, and vaccine responses. Lancet Infect Dis. 2009;9(8):493-504. Epub 2009/07/25. doi: 10.1016/s1473-3099(09)70175-6. PubMed PMID: 19628174; PubMed Central PMCID: PMCPMC2775097.
30. Arimori Y, Nakamura R, Yamada H, Shibata K, Maeda N, Kase T, et al. Type I interferon limits influenza virus-induced acute lung injury by regulation of excessive inflammation in mice. Antiviral Res. 2013;99(3):230-7. Epub 2013/06/01. doi: 10.1016/j.antiviral.2013.05.007. PubMed PMID: 23721943.
31. Jackson. B6(Cg)-Ifnar1tm1.2Ees/J, last excessed 10/08/2022: The Jackson Laboratory; 2022. Available from: https://www.jax.org/strain/028288.
32. Jackson. B6.129S7-Rag1tm1Mom/J, last excessed 10/08/2022: The Jackson Laboratory; 2022. Available from: https://www.jax.org/strain/002216.
33. Bissel SJ, Giles BM, Wang G, Olevian DC, Ross TM, Wiley CA. Acute murine H5N1 influenza A encephalitis. Brain Pathol. 2012;22(2):150-8. Epub 2011/07/01. doi: 10.1111/j.1750-3639.2011.00514.x. PubMed PMID: 21714828; PubMed Central PMCID: PMCPMC3204170.
34. Sonoguchi T, Sakoh M, Kunita N, Satsuta K, Noriki H, Fukumi H. Reinfection with influenza A (H2N2, H3N2, and H1N1) viruses in soldiers and students in Japan. J Infect Dis. 1986;153(1):33-40. Epub 1986/01/01. doi: 10.1093/infdis/153.1.33. PubMed PMID: 3941288.
35. Memoli MJ, Han A, Walters KA, Czajkowski L, Reed S, Athota R, et al. Influenza A Reinfection in Sequential Human Challenge: Implications for Protective Immunity and "Universal" Vaccine

675 Development. Clin Infect Dis. 2020;70(5):748-53. Epub 2019/04/07. doi: 10.1093/cid/ciz281. PubMed
676 PMID: 30953061; PubMed Central PMCID: PMCPMC7319262.
677 36. CDC. Background and Guidance on the Use of Influenza Antiviral Agents, last excessed
678 10/07/2022: Centers for Disease Control and Prevention; 2016. Available from:
679 https://www.cdc.gov/flu/professionals/antivirals/antiviral-use-influenza.htm.
680 37. FDA. Influenza (Flu) Antiviral Drugs and Related Information, last excessed 10/03/2022: U.S.
681 Food and Drug Administration; 2020. Available from: https://www.fda.gov/drugs/information-drug-
682 class/influenza-flu-antiviral-drugs-and-related-information.
683 38. Xiao X, Wang C, Chang D, Wang Y, Dong X, Jiao T, et al. Identification of Potent and Safe
684 Antiviral Therapeutic Candidates Against SARS-CoV-2. Front Immunol. 2020;11:586572. Epub
685 2020/12/17. doi: 10.3389/fimmu.2020.586572. PubMed PMID: 33324406; PubMed Central PMCID:
686 PMCPMC7723961.
687 39. Smith LE, D'Antoni D, Jain V, Pearce JM, Weinman J, Rubin GJ. A systematic review of factors
688 affecting intended and actual adherence with antiviral medication as treatment or prophylaxis in seasonal
689 and pandemic flu. Influenza Other Respir Viruses. 2016;10(6):462-78. Epub 2016/07/12. doi:
690 10.1111/irv.12406. PubMed PMID: 27397480; PubMed Central PMCID: PMCPMC5059947.
691 40. Tchesnokov EP, Obikhod A, Schinazi RF, Götte M. Delayed chain termination protects the anti-
692 hepatitis B virus drug entecavir from excision by HIV-1 reverse transcriptase. J Biol Chem.
693 2008;283(49):34218-28. Epub 2008/10/23. doi: 10.1074/jbc.M806797200. PubMed PMID: 18940786;
694 PubMed Central PMCID: PMCPMC2590697.
695 41. Kokic G, Hillen HS, Tegunov D, Dienemann C, Seitz F, Schmitzova J, et al. Mechanism of SARS-
696 CoV-2 polymerase stalling by remdesivir. Nat Commun. 2021;12(1):279. Epub 2021/01/14. doi:
697 10.1038/s41467-020-20542-0. PubMed PMID: 33436624; PubMed Central PMCID: PMCPMC7804290.
698 42. Fukao K, Ando Y, Noshi T, Kitano M, Noda T, Kawai M, et al. Baloxavir marboxil, a novel cap-
699 dependent endonuclease inhibitor potently suppresses influenza virus replication and represents
700 therapeutic effects in both immunocompetent and immunocompromised mouse models. PLoS One.
701 2019;14(5):e0217307. Epub 2019/05/21. doi: 10.1371/journal.pone.0217307. PubMed PMID: 31107922;
702 PubMed Central PMCID: PMCPMC6527232 Research, Co., Ltd, an affiliation of Shionogi. This does not
703 alter our adherence to PLOS ONE policies on sharing data and materials.
704 43. Wong ZX, Jones JE, Anderson GP, Gualano RC. Oseltamivir treatment of mice before or after
705 mild influenza infection reduced cellular and cytokine inflammation in the lung. Influenza Other Respir
706 Viruses. 2011;5(5):343-50. Epub 2011/06/15. doi: 10.1111/j.1750-2659.2011.00235.x. PubMed PMID:
707 21668689; PubMed Central PMCID: PMCPMC4942046.
708 44. Pizzorno A, Abed Y, Rhéaume C, Boivin G. Oseltamivir-zanamivir combination therapy is not
709 superior to zanamivir monotherapy in mice infected with influenza A(H3N2) and A(H1N1)pdm09 viruses.
710 Antiviral Res. 2014;105:54-8. Epub 2014/03/04. doi: 10.1016/j.antiviral.2014.02.017. PubMed PMID:
711 24583158.
712 45. Garigliany MM, Habyarimana A, Lambrecht B, Van de Paar E, Cornet A, van den Berg T, et al.
713 Influenza A strain-dependent pathogenesis in fatal H1N1 and H5N1 subtype infections of mice. Emerg
714 Infect Dis. 2010;16(4):595-603. Epub 2010/03/31. doi: 10.3201/eid1604.091061. PubMed PMID:
715 20350372; PubMed Central PMCID: PMCPMC3321946.
716 46. Gounder AP, Boon ACM. Influenza Pathogenesis: The Effect of Host Factors on Severity of
717 Disease. J Immunol. 2019;202(2):341-50. Epub 2019/01/09. doi: 10.4049/jimmunol.1801010. PubMed
718 PMID: 30617115; PubMed Central PMCID: PMCPMC6327976.
719 47. Iwasaki A, Medzhitov R. Control of adaptive immunity by the innate immune system. Nat Immunol.
720 2015;16(4):343-53. Epub 2015/03/20. doi: 10.1038/ni.3123. PubMed PMID: 25789684; PubMed Central
721 PMCID: PMCPMC4507498.
722 48. Chern YJ, Tai IT. Adaptive response of resistant cancer cells to chemotherapy. Cancer Biol Med.
723 2020;17(4):842-63. Epub 2020/12/11. doi: 10.20892/j.issn.2095-3941.2020.0005. PubMed PMID:
724 33299639; PubMed Central PMCID: PMCPMC7721100.
725 49. Stannard HL, Mifsud EJ, Wildum S, Brown SK, Koszalka P, Shishido T, et al. Assessing the fitness
726 of a dual-antiviral drug resistant human influenza virus in the ferret model. Commun Biol. 2022;5(1):1026.
727 Epub 2022/09/29. doi: 10.1038/s42003-022-04005-4. PubMed PMID: 36171475; PubMed Central

PMCID: PMCPMC9517990 employees of F. Hoffmann-La Roche. All other authors declare no competing interests.

50. Lee N, Chan PK, Hui DS, Rainer TH, Wong E, Choi KW, et al. Viral loads and duration of viral shedding in adult patients hospitalized with influenza. J Infect Dis. 2009;200(4):492-500. Epub 2009/07/14. doi: 10.1086/600383. PubMed PMID: 19591575; PubMed Central PMCID: PMCPMC7110250.

51. de Courville C, Cadarette SM, Wissinger E, Alvarez FP. The economic burden of influenza among adults aged 18 to 64: A systematic literature review. Influenza Other Respir Viruses. 2022;16(3):376-85. Epub 2022/02/06. doi: 10.1111/irv.12963. PubMed PMID: 35122389; PubMed Central PMCID: PMCPMC8983919.

52. Health WSDo. Are you at high risk for flu?, last excessed 10/08/2022. 2022.

53. CDC. Flu Symptoms & Complications, last excessed 10/06/2022. 2022.

54. CDC. HPAI A H5 Virus Background and Clinical Illness, last excessed 10/07/2022. 2015.

55. ECDC. Facts about avian influenza in humans, last excessed 10/10/2022: European Centre for Disease Prevention and Control; 2022. Available from: https://www.ecdc.europa.eu/en/avian-influenza-humans/facts.

56. Kiso M, Yamayoshi S, Murakami J, Kawaoka Y. Baloxavir Marboxil Treatment of Nude Mice Infected With Influenza A Virus. J Infect Dis. 2020;221(10):1699-702. Epub 2019/12/15. doi: 10.1093/infdis/jiz665. PubMed PMID: 31837268; PubMed Central PMCID: PMCPMC7184910.

57. Kimura K, Adlakha A, Simon PM. Fatal case of swine influenza virus in an immunocompetent host. Mayo Clin Proc. 1998;73(3):243-5. Epub 1998/03/25. doi: 10.4065/73.3.243. PubMed PMID: 9511782.

58. Neumann G, Watanabe T, Ito H, Watanabe S, Goto H, Gao P, et al. Generation of influenza A viruses entirely from cloned cDNAs. Proc Natl Acad Sci U S A. 1999;96(16):9345-50. Epub 1999/08/04. PubMed PMID: 10430945; PubMed Central PMCID: PMC17785.

59. Nogales A, Ávila-Pérez G, Rangel-Moreno J, Chiem K, DeDiego ML, Martínez-Sobrido L. A Novel Fluorescent and Bioluminescent Bireporter Influenza A Virus To Evaluate Viral Infections. J Virol. 2019;93(10). Epub 2019/03/15. doi: 10.1128/jvi.00032-19. PubMed PMID: 30867298; PubMed Central PMCID: PMCPMC6498038.

60. Carey MF, Peterson CL, Smale ST. The primer extension assay. Cold Spring Harb Protoc. 2013;2013(2):164-73. Epub 2013/02/05. doi: 10.1101/pdb.prot071902. PubMed PMID: 23378648.

Figure captions

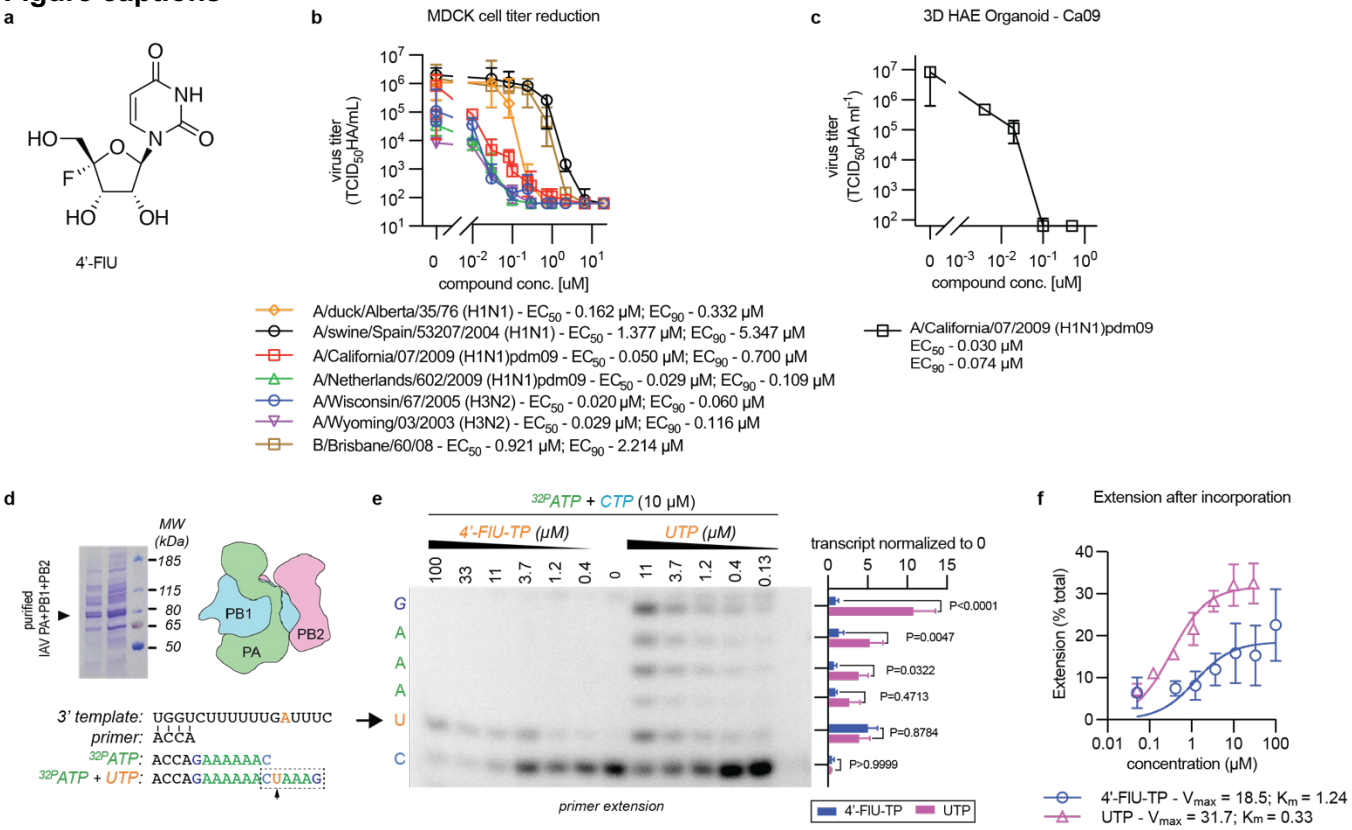

Figure 1: *In vitro* potency and MOA of 4'-FIU against influenza viruses. **a)** Structure of 4'-FIU. **b)** Dose-response assay of 4'-FIU on MDCK cells. Cells were infected with different subtype IAV or with an IBV isolate. Lines represent 4-parameter variable slope regression model, symbols show data median with 95% CI (n=3); EC_{50} and EC_{90} values are given. **c)** Dose-response assay of 4'-FIU on a well-differentiated HAE organoid against Ca09. Compound was added to the basolateral chamber; line connects data median of apically shed virus, error bars represent 95% CI; EC_{50} and EC_{90} values are shown; n=3. **d)** Coomassie blue staining of purified recombinant IAV RdRP proteins after gel electrophoresis and RNA template sequences used in primer extension assays. **e)** *In vitro* RdRP assay in the presence of ^{32}P-ATP, CTP, and UTP or 4'-FIU-TP as indicated. Representative autoradiogram showing the sequence section highlighted by dashed box in (d); the first incorporation of UTP or 4'-FIU-TP is after position *i*=8 of the amplicon (arrow). The sequence of the amplicon and results of phosphoimager-quantitation of relative signal intensities observed in the presence of 11 µM UTP or 4'-FIU-TP are specified to the left and right of the autoradiogram, respectively. Quantitation graph shows mean values of independent experiments (n=3) ± SD; analysis with 1-way ANOVA with Dunnett's *post*

hoc test; P values are shown in the graph. Uncropped autoradiogram and replicates are provided in (S2 Fig). **f)** Kinetic analysis of 4'-FIU-TP and UTP incorporation into the amplicon shown in (e) and (S2 Fig). Lines represent non-linear regression kinetics with Michaelis-Menten model, K_m and V_{max} are shown, error bars represent 95% CI.

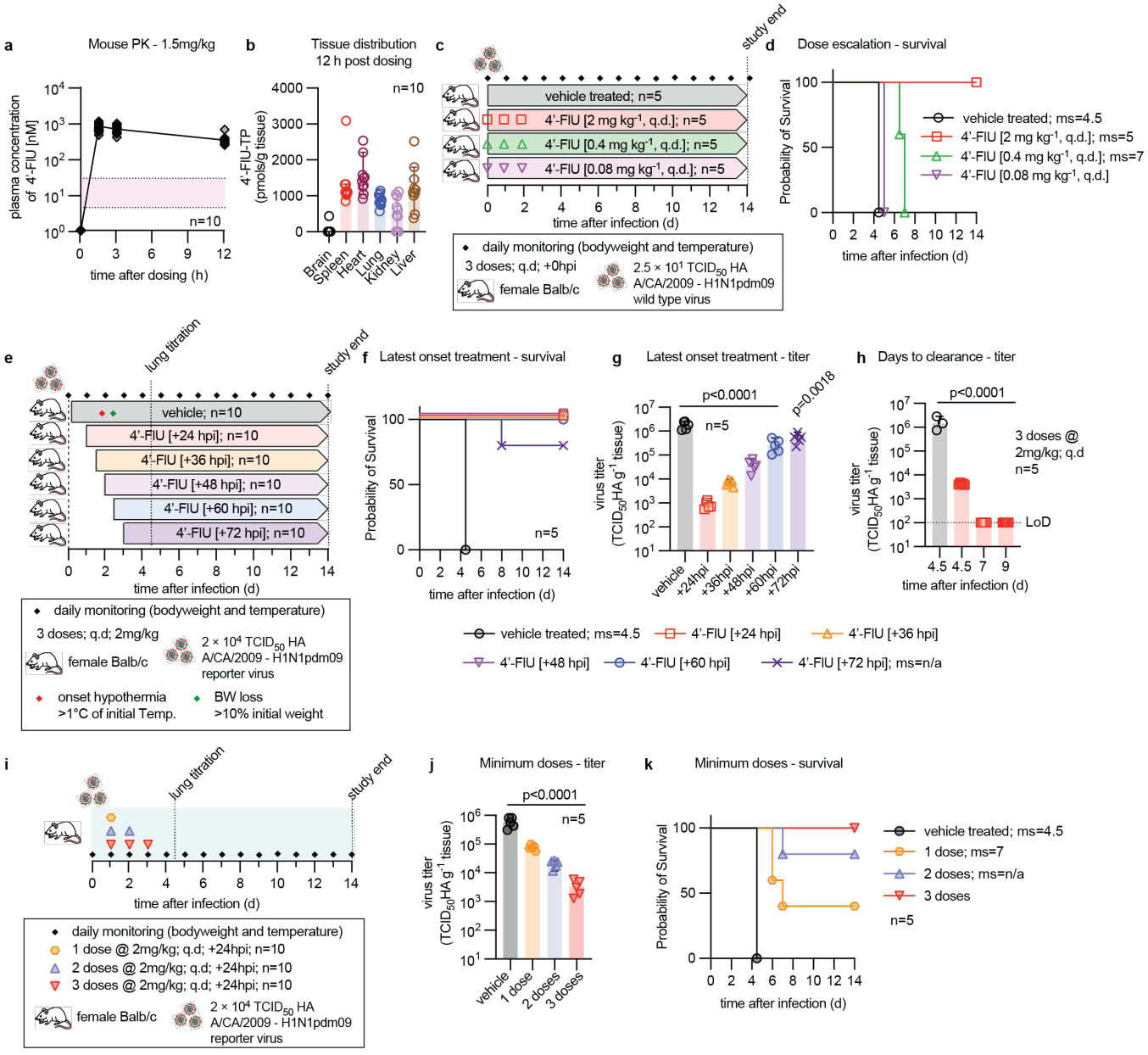

Figure 2: Treatment paradigms of 4'-FIU in mice. **a)** Mouse plasma exposure after a single oral dose of 1.5 mg/kg bodyweight. The red area denotes cell culture $EC_{90} \pm 1 \times SD$ against WSN, all donors as shown in (S1 Fig). **b)** Tissue distribution of bioactive anabolite 4'-FIU-TP in animals shown in (a) 12 hours after dosing. **c)** Schematic of dose-to-failure study against standard recA/CA/2009 (H1N1). **d)**

Survival of animals treated as specified in (c). Median survival (ms) time in days is specified; Kaplan-Meier simple survival analysis. **e)** Study schematic to determine the therapeutic time window of oral 4'-FlU in mice, using recA/CA/2009-maxGFP-HA (H1N1) as viral target. **f)** Survival of animals treated as specified in (e). Median survival (ms) time in days is specified; Kaplan-Meier simple survival analysis. **g)** Lung viral load of a set of animals treated as in (e) was determined 4.5 days after infection. **h)** Time-to-viral-clearance study. Mice were infected and treated with 4'-FlU at 2 mg/kg starting 24 hours after infection and continued q.d. Lung virus load was determined in vehicle-treated animals 4.5 days after infection, and in 4'-FlU-treated animals 4.5, 7, and 9 days after infection. **i)** Schematic of minimal-number-of-doses finding study. **j)** Lung viral load of animals treated as in (i), determined 4.5 days after infection. **k)** Survival of a set of animals treated as in (i). Median survival (ms) time in days is specified; Kaplan-Meier simple survival analysis. Columns in (b, g, h, j) represent data medians with 95% CI, symbols specify individual animals; statistical analysis in (g, h, j) with 1-way ANOVA with Dunnett's *post hoc* test.

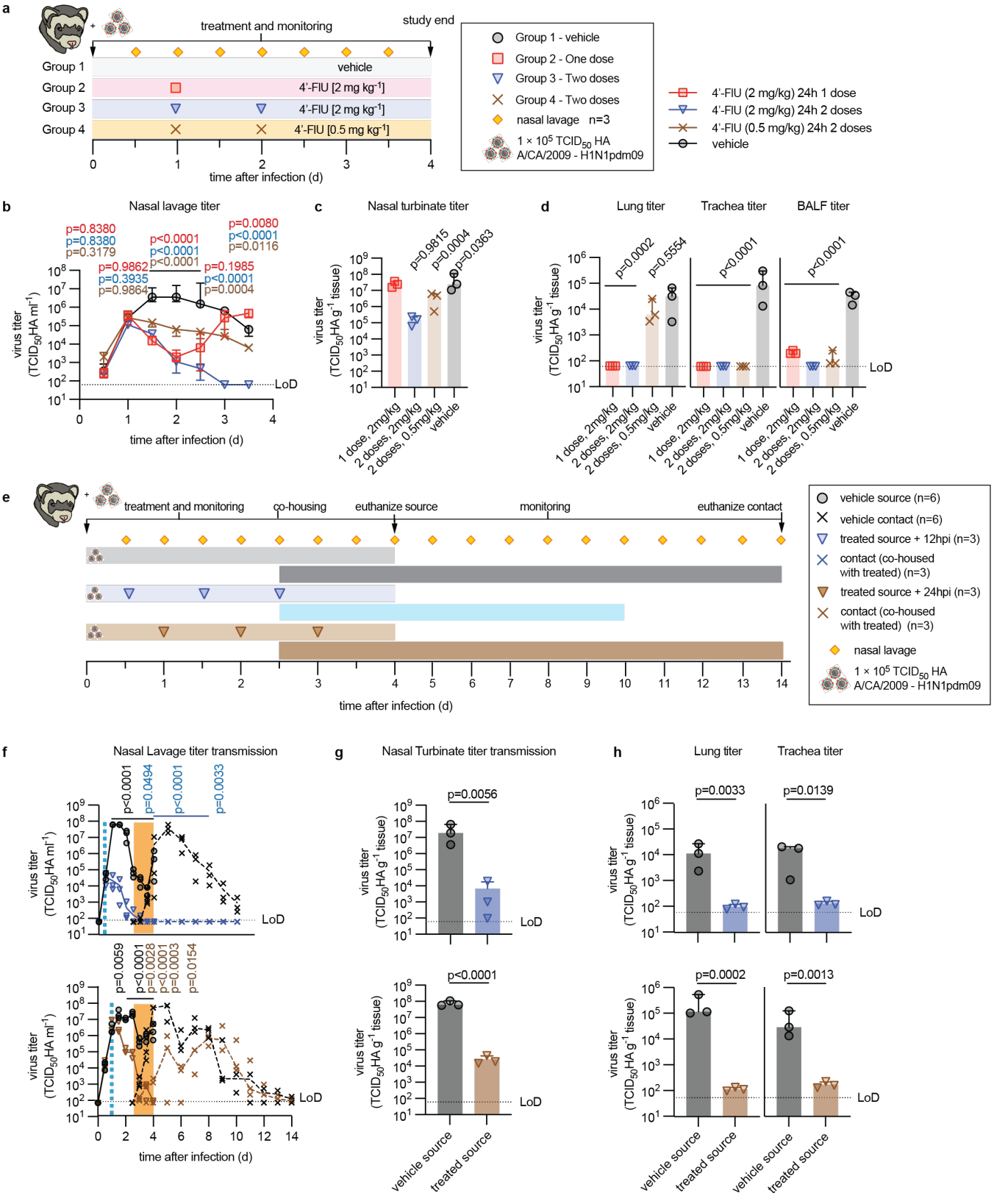

Figure 3: *In vivo* efficacy of 4'-FIU in the ferret transmission model. **a)** Ferret efficacy study schematic. **b)** Ferret shed viral titers in nasal lavages. Symbols represent data medians with 95% CI; 2-way ANOVA with Tukey's *post hoc* test, P values are specified; n=3. **c-d)** Tissue and BALF viral titers determined 4 days after infection. Columns represent data medians with 95% CI, symbols specify individual animals; 1-way ANOVA with Dunnett's *post hoc* test, P values are specified. **e)** Transmission study schematic. Treatment of source ferrets was started 12 or 24 hours after infection, animals were co-housed with untreated contact ferrets 2.5 days after infection. **f)** Ferret shed viral titers in nasal lavages of source animals and their sentinels. Light blue dashed line marks time of treatment onset; orange box highlights co-housing period. Symbols represent data medians with 95% CI; 2-way ANOVA with Tukey's *post hoc* test, P values are specified (P values in black compare source animals, P values in blue and brown compare contact ferrets). **g-h)** Virus load in nasal turbinates (g) and lung and trachea tissues (h) in source animals, collected 4 days after infection, respectively. Columns represent data medians with 95% CI; symbols show individual animals; unpaired t-test, P values are specified.

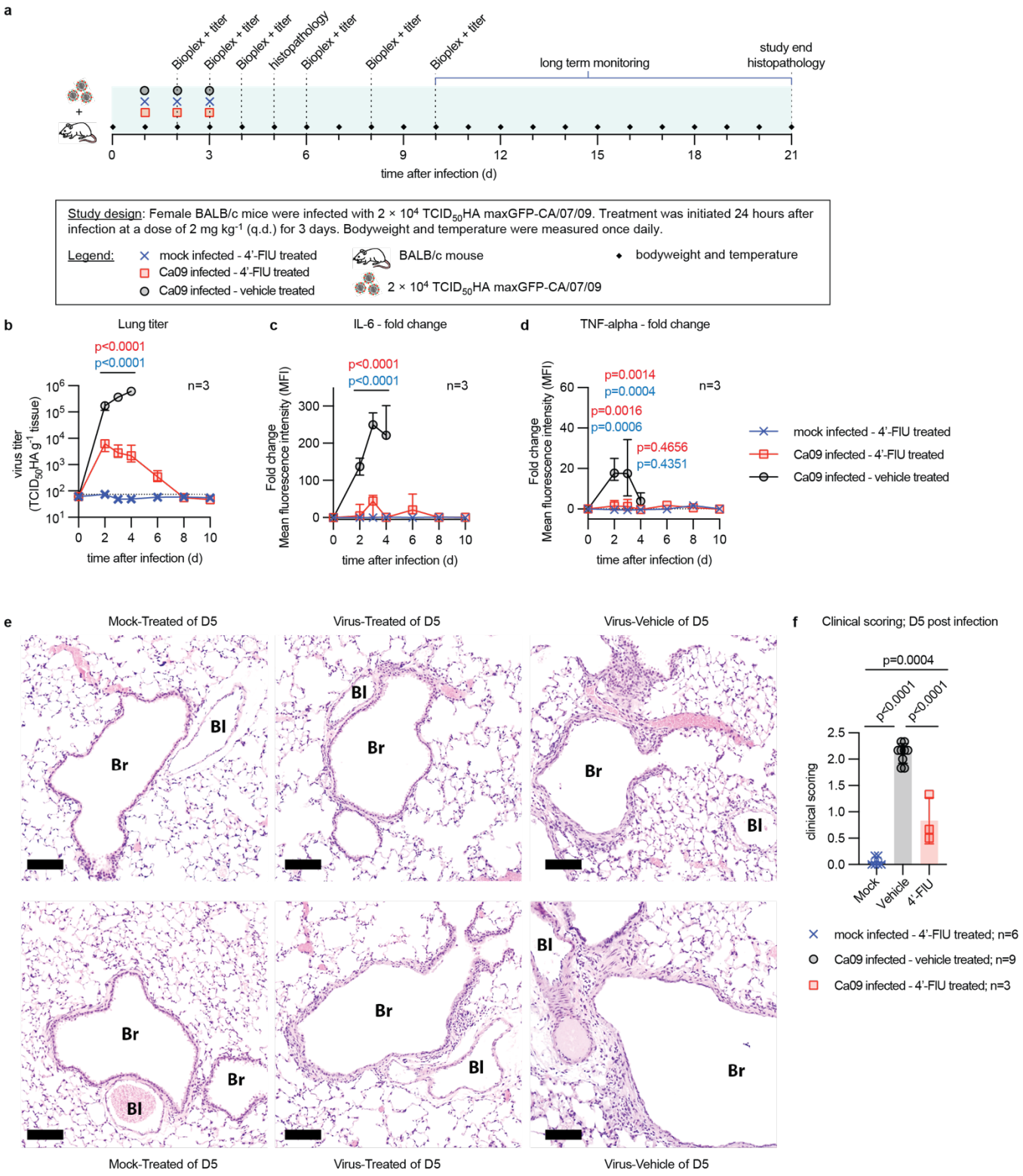

Figure 4: Effect of 4'-FIU on the antiviral immune response and lung histopathology. **a)** *In vivo* Bioplex and histopathology study schematic. **b)** Lung viral titers in animals treated as in (a). **c-d)** Changes in IL-6 (c) and TNF-α (d) levels present in BALF of animals treated as in (a), relative to levels at time of infection. Symbols in (b-d) represent data medians with 95% CI; 2-way ANOVA with Tukey's *post hoc*

test; P values are shown. **e)** Representative photomicrographs of lung tissue extracted 5 days after infection of animals treated as in (a). Tissues of two individual animals per study arm are shown at 10× magnification; scale bar denotes 100 µm; Br, Bronchiole; Bl, Blood vessel. **f)** Histopathology scores of animals treated as in (a). Lungs were extracted 5 days after infection. Scores for each animal represents a mean of individual alveolitis, bronchiolitis, vasculitis, pleuritis, perivascular cuffing (PVC), and interstitial pneumonia (IP) scores. Columns represent data medians with 95% CI; symbols show mean scores for each individual animal; 1-way ANOVA with Dunnett's *post hoc* test, P values and n values for each study arm are specified.

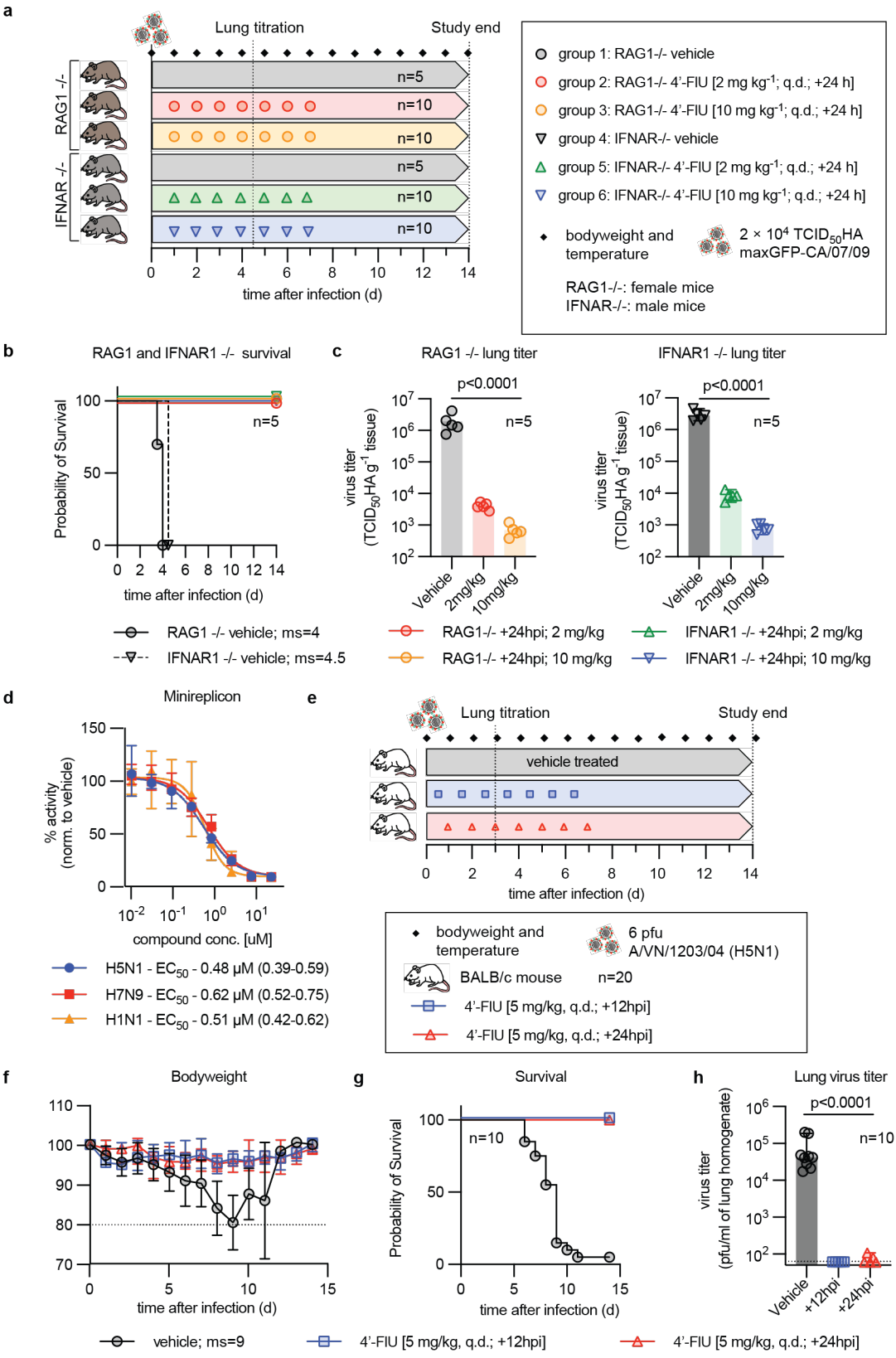

Figure 5: Efficacy of 4'-FlU in an immunocompromised host and against HPAI. **a)** Efficacy study schematic in immunocompromised mice, lacking B and T cells (RAG1 KO) or IFN1 receptor function

(IFNar1 KO). **b)** Survival study of animals treated as shown in (a). Median survival (ms) time in days is specified; Kaplan-Meier simple survival analysis. **c)** Lung viral load in animals from (a), determined 4.5 days after infection. Columns represent data medians with 95% CI; symbols show individual animals; 1-way ANOVA with Dunnett's *post hoc* test, P values are specified. **d)** Dose-response minigenome assay with RdRP complexes derived from IAV subtypes H1N1, H5N1, and H7N9. Lines represent 4-parameter variable slope regression models; symbols show data medians with 95% CI; n=3. EC_{50} concentrations and 95% CI are specified. **e)** Efficacy study schematic of 4'-FIU against HPAI H5N1. **f)** Body weight measurements of animals shown in (e). Symbols represent data means ± SD, normalized to animal body weight at study start. **g)** Survival study of animals infected with HPAI and treated as shown in (e). Median survival (ms) time in days is specified; Kaplan-Meier simple survival analysis. **h)** Lung virus load on day 3 after infection. Columns represent data medians with 95% CI; symbols show individual animals; 1-way ANOVA with Dunnett's *post hoc* test; P values and n values are specified.

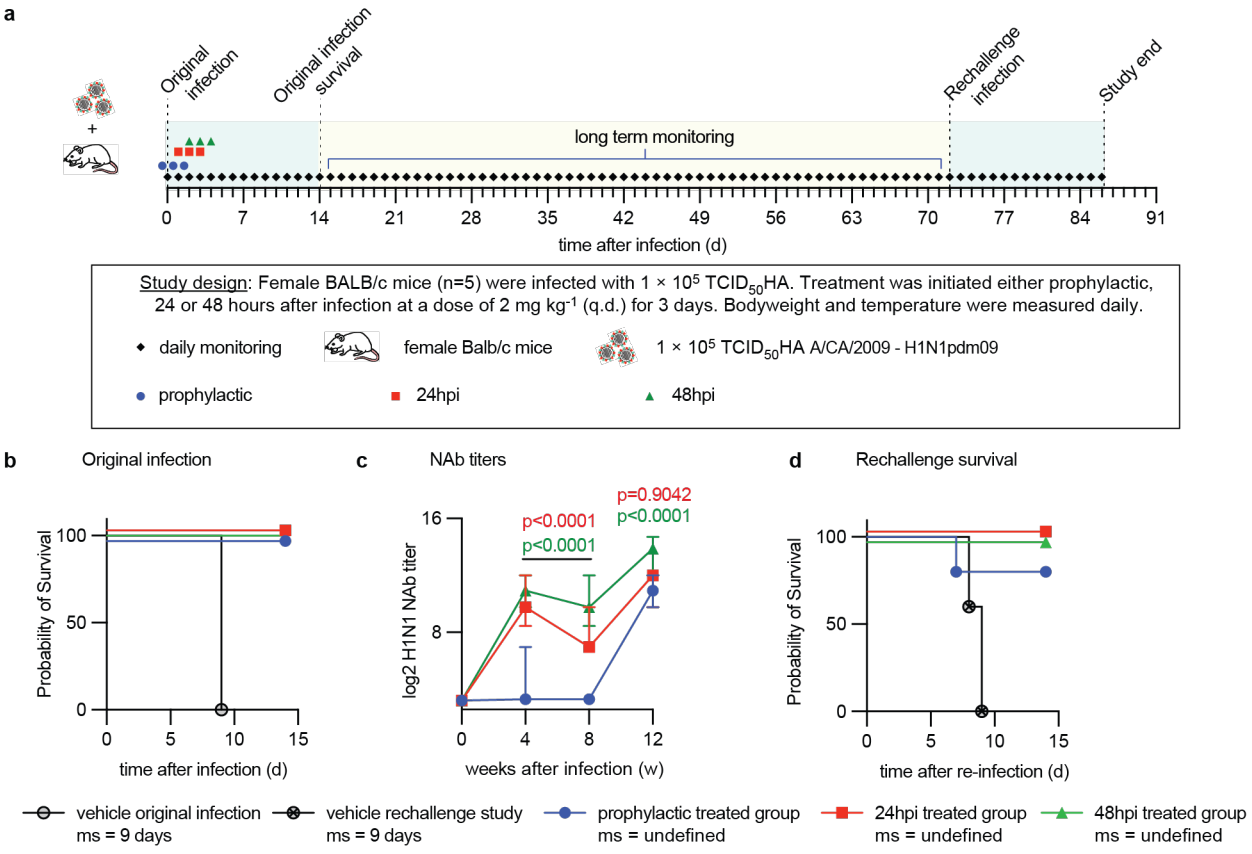

Figure 6: Reinfection of 4'-FIU-experienced animals with homotypic H1N1. **a)** Schematic of the treatment and reinfection study. For infection and reinfection, mice received aerosolized Ca09. **b)**

Survival study of animals infected, treated, and reinfected as shown in (a). Median survival (ms) time in days is specified; Kaplan-Meier simple survival analysis. **c)** Anti-H1N1 neutralizing antibody (nAb) titers developing in animals from (a). Symbols represent data medians with 95% CI; 2-way ANOVA with Tukey's *post hoc* test; P values are specified. **d)** Survival of animals after re-infection. Median survival (ms) time in days is specified; Kaplan-Meier simple survival analysis. N numbers for animals in (a-d) are specified in (a).